Structural and Chemical Changes of the P_M Intermediate of *Paracoccus denitrificans* Cytochrome *c* Oxidase Revealed by IR Spectroscopy with Labeled Tyrosines and Histidine†

Masayo Iwaki,‡ Anne Puustinen,§,|| Mårten Wikström,§ and Peter R. Rich*,‡

Glynn Laboratory of Bioenergetics, Department of Biology, University College London, Gower Street, London WC1E 6BT, U.K., and Helsinki Bioenergetics Group, Programme for Structural Biology and Biophysics, Institute of Biotechnology, University of Helsinki, PB 65 (Viikinkaari 1), FI-00014 University of Helsinki, Helsinki, Finland

Received June 5, 2006; Revised Manuscript Received July 17, 2006

ABSTRACT: Structural and chemical changes in the P_M intermediate of *Paracoccus denitrificans* cytochrome *c* oxidase have been investigated by attenuated total reflection-Fourier transform infrared spectroscopy. Prior studies of P_M *minus* oxidized (O) IR difference spectra of unlabeled, universally ^{15}N-labeled and ring-d_4-tyrosine-labeled proteins (Iwaki, M., Puustinen, A., Wikström, M., and Rich, P. R. (2004) *Biochemistry 43*, 14370−14378). provided a basis for band assignments to changes in metal centers and the covalently linked His−Tyr ligand of Cu_B and highlighted a structural alteration of the protonated Glu278 in the P_M intermediate. This work has been extended to equivalent measurements on enzymes with $^{13}C_9{}^{15}N$-labeled and ring-$^{13}C_6$-labeled tyrosine and with $^{13}C_6{}^{15}N_3$-labeled histidine. Histidine labeling allows the assignment of troughs at 1104 and 973 cm^{-1} in reduced *minus* O spectra to histidine changes, whereas tyrosine labeling moves otherwise obscured tyrosine bandshifts to 1454−1437 and 1287−1284 cm^{-1}. P_M *minus* O spectra reveal bands at 1506, 1311, and 1094 cm^{-1} in the oxidized state that are replaced by a band at 1519 cm^{-1} in P_M. These bands shift with both tyrosine- and histidine-labeling, providing evidence for their assignment to the covalent His−Tyr and for its chemical change in P_M. Comparisons of isotope effects on the amide I regions in P_M *minus* O spectra demonstrate that amide carbonyl bonds of tyrosine and histidine are major contributors. This suggests a structural alteration in P_M that is centered on the His276−Pro277−Glu278−Val279−Tyr280 pentapeptide formed by the His−Tyr covalent linkage. This structural change is proposed to mediate the perturbation of the IR band of the protonated Glu278 headgroup.

Atomic resolution structures of mitochondrial and bacterial cytochrome *c* oxidases (*1*−*3*) have provided a wealth of structure/function information. Nevertheless, major questions remain as to the chemical nature of important intermediates and the sites and dynamics of the associated protonation changes that provide the coupling mechanism. Two central intermediates are the 607 nm (610 nm in *Paracoccus denitrificans*) peroxy (P)[1] and 580 nm ferryl (F) intermediates that are formed transiently in the forward reaction of fully reduced cytochrome *c* oxidase with oxygen (*4*, *5*). A 607 nm state can also be formed as a relatively stable species by the reaction of oxidized enzyme at high pH with CO and oxygen (*6*). This species has been termed P_M to distinguish it from a related 607 nm form, P_R, which is formed transiently when oxygen reacts with the fully reduced enzyme (*7*−*10*). Alternatively, both P_M and F can be formed by the reaction of oxidized enzyme with H_2O_2; the reaction with the first H_2O_2 produces P_M, and this reacts with a second H_2O_2 to produce F (*11*−*13*).

In both P_M and F, the O−O bond is broken, and heme a_3 is in the ferryl state (*14*−*19*). This O−O bond breakage requires four electrons. In the case of P_M formation, only two electrons have been donated into the enzyme from external sources. The third electron is provided by the formation of the ferryl state of heme a_3, and the fourth is thought to arise from a site within the protein that can form a radical, although one is not observed by EPR spectroscopy. However, the radical is most likely located primarily on the covalent His−Tyr ligand to Cu_B (*2*, *20*, *20*−*24*), and spin coupling with $Cu_B{}^{2+}$ could account for its EPR silence (*25*, *26*). The transient P_R state observed in flow/flash studies of fully reduced oxidase differs from P_M because the radical site is either not formed or is re-reduced rapidly by electron transfer from ferrous heme *a*; subsequent proton uptake converts P_R to the F intermediate (*7*−*10*).

Fourier-transform infrared (FTIR) transmission spectroscopy, in combination with electrochemical and photochem-

† This work was funded by grants from the BBSRC (grant code BBC51715X1 to P.R.R.) and the Academy of Finland (programs 44895 and 42739 to M.W. and A.P.).

* To whom correspondence should be addressed. Tel: (+44) 20 7679 7746. Fax: (+44) 20 7679 7096. E-mail: prr@ucl.ac.uk.

‡ University College London.

§ University of Helsinki.

|| Present address: Finnish Institute of Occupational Health, Topeliuksenkatu 41, 00250 Helsinki, Finland.

[1] Abbreviations: (ATR)-FTIR spectroscopy, (attenuated total reflection)-Fourier transform infrared spectroscopy; O, fully oxidized; R, fully reduced; P, 607 nm species; P_M, a stable P species formed when mixed-valence enzyme reacts with oxygen; P_R, a transient P species with one more electron in the vicinity of the binuclear center in comparison to that of P_M; F, a 580 nm ferryl species that is isoelectronic with P_R.

10.1021/bi061114b CCC: $33.50 © 2006 American Chemical Society
Published on Web 08/18/2006

ical techniques, has been used extensively to probe redox- and ligand-induced structural changes in individual cofactors and amino acids in cytochrome *c* oxidase and related oxidases (*27*−*35*). Attenuated Total Reflection (ATR)-FTIR spectroscopy (*36*, *37*) has provided access to the IR features of the P_M and F intermediates of bovine and bacterial oxidases (*38*−*40*). Effects of H/D exchange (*39*), ring-d_4-tyrosine- (*41*) and universal ^{15}N-labeling (*42*) were used to aid interpretation of details of the P_M *minus* O spectra. These studies are extended here to effects of $^{13}C_9{}^{15}$N-labeled and ring-$^{13}C_6$-labeled tyrosine and $^{13}C_6{}^{15}N_3$-labeled histidine.

MATERIALS AND METHODS

Mutagen Mutagenesis. To construct a histidine auxotroph in *P. denitrificans* MR3 strain (*43*), an overnight culture was diluted into LB medium (optical density at 690 nm of 0.2−0.3) and grown with aeration for 2.5 h to an OD_{690} of 0.9 before treatment with the mutagen N-methyl-N′-nitro-N-nitrosoguanidine (50 μg/mL) for 15 min (*44*). Enrichment of mutants was achieved by growing mutagenized cells that had been diluted 1:10 and left overnight on succinate minimal medium for 3 h to an OD_{690} of 0.9, after which time the cells were incubated with penicillin (16 mg/mL) for 1 h. Six mutants unable to grow without added histidine in succinate minimal media were found from 3000 colonies.

Bacterial Growth and Enzyme Purification. P. denitrificans was grown in succinate minimal media (*45*). For universal ^{15}N-labeling growth media contained ^{15}N-ammonium chloride (ICON Isotopes) as the sole nitrogen source. Labeling with $^{13}C_9{}^{15}$N-, ring-$^{13}C_6$- and ring-d_4-labeled tyrosines (ICON Isotopes) was achieved as described in ref 46 (*46*). Then 40 mg/L of $^{13}C_6{}^{15}N_3$-labeled histidine (ICON Isotopes, 98:98 atom%) was used in the growth medium and a labeling extent of 99% was estimated by mass spectrometry analysis of the isolated enzyme. Purified cytochrome *c* oxidase (*47*) was dissolved in 20 mM TRIS-HCl and 0.05% w/v β-dodecyl maltoside at pH 7.8 and stored at 77 K until required.

Film Preparation. Production of stable films for ATR-FTIR measurements required the depletion of detergent content so that the sample became sufficiently hydrophobic. The preparation of ATR-ready materials and rehydrated film on the ATR prism (3-mm diameter silicon, 3-bounce, SensIR Europe) were essentially as described previously (*39*, *48*). In brief, 10−20 μL of oxidase (100−200 μM stock) was diluted in 20 mM potassium phosphate buffer at pH 8.0 and pelleted by centrifugation. The pellet was homogenized in the same buffer containing 0.01% w/v sodium cholate and 0.01% w/v octyl glucoside and again pelleted by centrifugation. This was repeated four times with detergent-free 20 mM phosphate buffer and finally with 1 mM phosphate buffer. The resultant ATR-ready material was dispersed in 5 μL of distilled water and deposited on the ATR prism. After drying with a gentle stream of N_2 gas, the protein film was rehydrated with a buffer solution (50 mM CHES, 50 mM potassium phosphate, 200 mM KCl at pH 9.0).

For exchange into deuterium oxide (D_2O), all buffers for the preparation of ATR-ready material and its rehydration were prepared in D_2O at the required pD as described previously (*39*) and assuming pD = pH meter reading + 0.4 (*49*).

Visible Spectra During Reduction/Oxidation and Intermediate Formation. The rehydrated film was covered by a chamber that allowed buffers to be perfused over the film surface and visible absolute and difference absorption changes to be recorded synchronously with IR changes, as detailed in (*38*, *39*). Quantitation of forms was assessed from visible spectra using the relative extinction coefficients given for bovine oxidase in (*50*) and assuming that the P_M spectrum of *P. denitrificans* oxidase is uniformly red-shifted by 3 nm relative to bovine oxidase. As described in previous work, oxidase films were scanned with a visible beam in the 500−700 nm range versus a clean prism surface as background to produce absolute visible spectra. The resulting fully reduced (R) *minus* oxidized (O) difference spectra exhibited the characteristic peak at 606 nm. Quantitation versus absolute spectra indicated that more than 90% of the sample was redox-active. For generation of the P_M intermediate, background spectra of the fast oxidized form were recorded, and the buffer was changed to one that had been bubbled briefly with CO gas. All forms over several minutes developed a band in their difference spectra at 610 nm that is characteristic of the P_M intermediate (*39*) and quantitation versus reduced *minus* oxidized difference spectra indicated 70−90% conversion to P_M in all cases (data not shown).

IR Difference Spectra. ATR-FTIR spectra were recorded with a Bruker ISF 66/S spectrometer fitted with a liquid nitrogen-cooled MCT-A detector. All frequencies quoted have an accuracy to ± 1 cm^{-1}. Degassed buffer (50 mM CHES, 50 mM potassium phosphate and 200 mM KCl) at pH 9.0 or pD 9.0 (*39*) was used as perfusant throughout. In order to ensure that the oxidase was in the fast oxidized state (*51*, *52*), a cycle of reduction and reoxidation of the protein film was first performed by perfusion with buffer containing 3 mM sodium dithionite followed by one containing 1 mM potassium ferricyanide. The ferricyanide-containing buffer was then switched to buffer alone to minimize ferricyanide contributions to R *minus* O IR and visible spectra. To measure P_M *minus* O spectra, a reference spectrum of the oxidized state was recorded during perfusion with buffer at pH 9.0 containing 0.2 mM ferricyanide. Generation of P_M was then induced by switching to an identical aerobic buffer that had been bubbled briefly with CO. Because of the difficulty of CO removal from samples that had been exposed to CO/oxygen, new samples were used for each run, and spectra from 6−8 different samples were averaged (equivalent to 160 000−220 000 for R *minus* O or 24 000−32 000 for P_M *minus* O, averaged interferograms) to produce the spectra shown. All measurements were made at room temperature with a flow rate of 1.5 mL/min.

Sample Quality Control. As in previous studies (*39*, *48*), sample integrity at the end of the experiment was assessed by the generation of the CO-ligated reduced state by perfusion with buffer containing dithionite and CO. The CO stretch band region was deconvoluted into a set of Gaussian components in order to assess the percentage of the α form in which the CO ligated to ferrous heme a_3 iron has a C−O stretch frequency of 1965 cm^{-1} with a halfpeak width of 7 cm^{-1}. All oxidase samples also contain smaller amounts of broader β forms (*53*), whose structural variance remains unclear. In our preparations, the levels of these β forms were independent of pH and always less than 25% of the total integrated area.

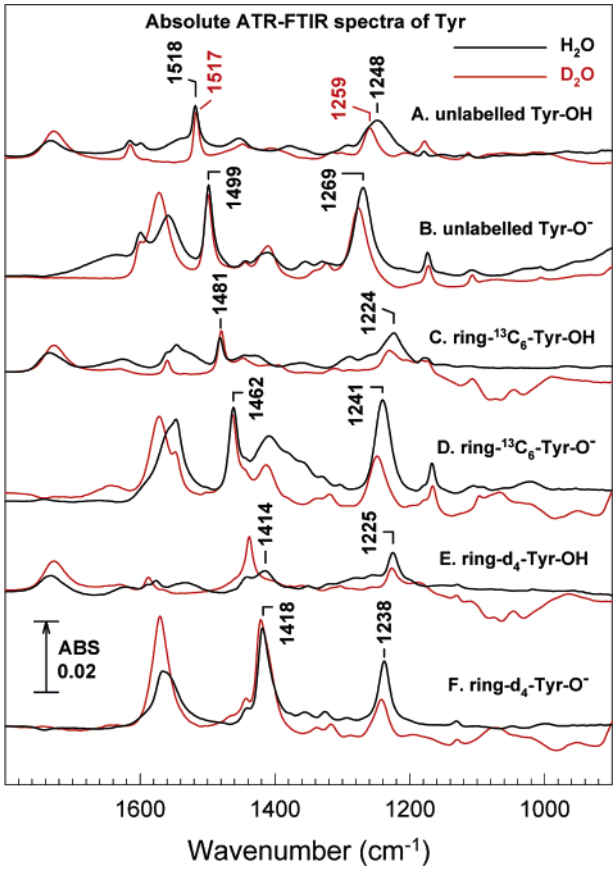

FIGURE 1: Absolute ATR-FTIR spectra of tyrosine. Absolute ATR-FTIR spectra of neutral (A, C and E) and deprotonated forms (B, D and F) of unlabeled (A and B), ring-$^{13}C_6$-labeled (C, D) and ring-d_4-labeled (E, F) tyrosine (100 mM) were measured in 1 M HCl or NaOH (black) or 1 M DCl or NaOD (red). For quantitative purposes, the 0.02 ΔA scale bar is equivalent to an extinction coefficient of 467 $M^{-1}\cdot cm^{-1}$ at 1400 cm^{-1}. (The values for other frequencies may be calculated from its direct proportion to wavenumber.)

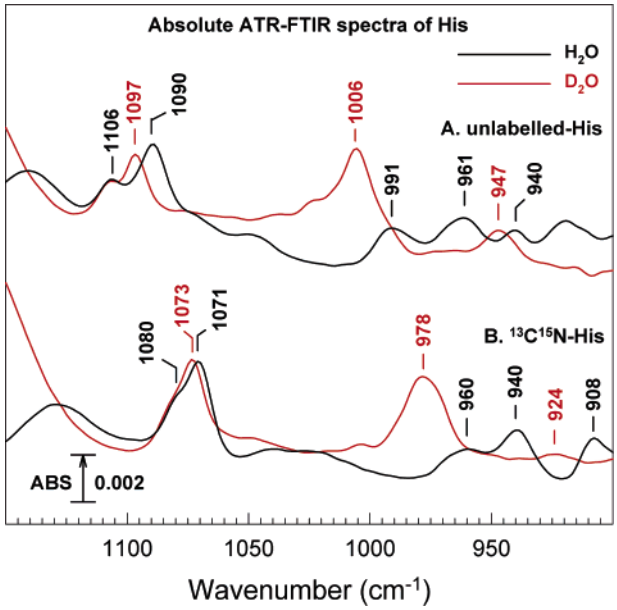

FIGURE 2: Absolute ATR-FTIR spectra of histidine. Absolute ATR-FTIR spectra of the imidazole form of unlabeled (A) and $^{13}C_6{}^{15}N_3$-labeled (B) histidines (200 mM) were measured in H_2O (black) or D_2O (red) media. Sample pH/D had been adjusted to pH 7.5 and pD 8.0 for unlabeled histidine and pH 8.0 and pD 8.1 for labeled histidine.). For quantitative purposes, the 0.002 ΔA scale bar is equivalent to an extinction coefficient of 17 $M^{-1}\cdot cm^{-1}$ at 1000 cm^{-1}. (The values for other frequencies may be calculated from its direct proportion to wavenumber.)

RESULTS AND DISCUSSION

Isotope Effects on Model Tyrosine and Histidine Spectra. Absolute ATR-FTIR spectra of L-tyrosines and L-histidines were measured with the same ATR prism in both H_2O and D_2O media to provide reference data for analyses of the protein spectra. Tyrosine (Sigma-Aldrich) and its isotopic forms (Icon Isotopes) were dissolved to 100 mM in 1 M H(D)Cl or 1 M NaOH(D). Unlabeled histidine (Sigma-Aldrich) and $^{13}C_6{}^{15}N_3$-His (Icon Isotopes) were dissolved to 200 mM in distilled water or deuterium oxide (D_2O) to which NaOH(D) or H(D)Cl had been added to provide the required pH/pD. A 10 μL aliquot of each sample was placed on the prism, and absolute absorption spectra were recorded (each the average of 1000 interferograms). In all cases, the spectra of solvent were recorded separately and subtracted to produce the spectra shown.

Figure 1 shows spectra of tyrosine and tyrosinate variants in both H_2O and D_2O media. These vibrational spectra are well understood in terms of contributions from the amino and carboxylic amino acid moieties, together with the bands arising from the functional headgroup (*54*−*57*). Spectra of the fully labeled $^{13}C_9{}^{15}N$ material have been omitted because the additional effects on the carboxylic and amino groups are not relevant here. The key features to note in relation to the present analyses are the downshifts of the Tyr-OH υ(CC) and υ(CO), υ(CC) bands from 1518 and 1248 cm^{-1} (Figure 1A) to 1481 and 1224 cm^{-1} in ring-$^{13}C_6$-labeled (Figure 1C), and to 1414 and 1225 cm^{-1} in ring-d_4-labeled (Figure 1E) tyrosines. Similar shifts are seen in D_2O media. The equivalent bands of the tyrosinate forms that are labeled in Figure 1 have similar isotope shift patterns (Figure 1B, D, and F).

Absolute IR properties of the neutral imidazole form of histidine are shown in Figure 2. The solution spectra of the imidazole forms are complicated because there is an equilibrium mixture of species protonated at the N_π or N_τ nitrogen. Key bands in relation to the present work are those arising primarily from the C5N1 ($C5N_\tau$) stretch at 1106 cm^{-1} (N_π protonated) and 1090 cm^{-1} (N_τ protonated) and more complex ring modes at 991 and 961 cm^{-1} (Figure 2A). These bands and other primary features of all three protonated forms of the headgroup, together with the shifts on deuteration, are well documented (*54*, *57*−*59*). All four of these bands are, as expected, strongly downshifted in $^{13}C_6{}^{15}N_3$-labeled histidine to, respectively, 1080, 1071, 960, and 940 cm^{-1} (Figure 2B). Such isotopic shifts have been exploited to provide some of the assignments in the protein spectra described below.

Reduced Minus Oxidized IR Difference Spectra

Fully reduced (R) *minus* oxidized (O) IR difference spectra at pH 9.0 were recorded by re-reduction after an initial reduction/reoxidation cycle to ensure that the proteins were in the fast, unligated state (*52*) as described previously (*48*). An overview of the resulting set of spectra is presented in Supporting Information (Figure S1). For ease of comparison,

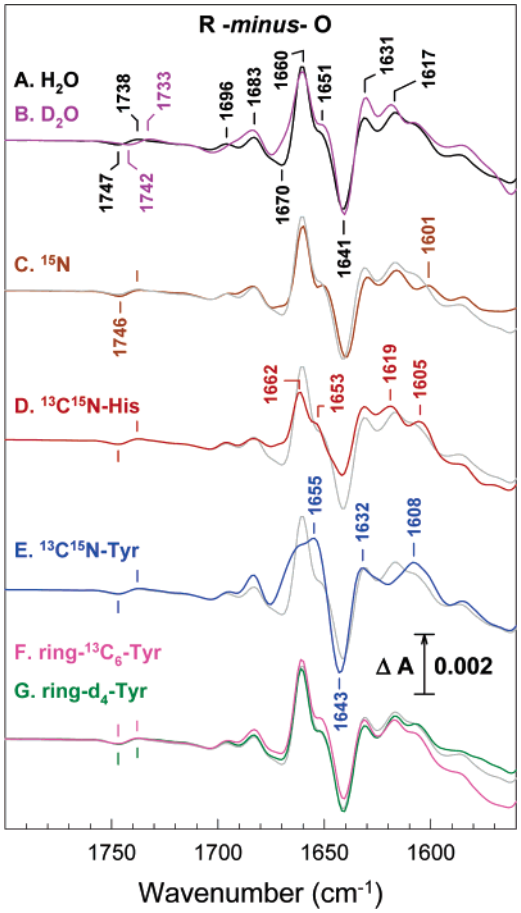

FIGURE 3: Isotope effects on the 1800−1560 cm^{-1} region of R *minus* O difference spectra. Spectra were recorded as described in Materials and Methods, with transitions between fully reduced and oxidized states induced by alternating perfusion of a buffer containing 3 mM sodium dithionite with an aerobic buffer. All isotopically labeled enzymes were measured in H_2O media. Spectra are unlabeled in H_2O buffer (A, black) or D_2O buffer (B, purple), universal ^{15}N-labeled (C, brown), $^{13}C_6{}^{15}N_3$-histidine-labeled (D, red), $^{13}C_9{}^{15}N$-tyrosine-labeled (E, blue), ring-$^{13}C_6$-tyrosine-labeled (F, pink), and ring-d_4-tyrosine-labeled (G, green) forms at pH/D 9.0. Typically, the spectra shown are averages of 50−60 redox cycles, each an average of 2000 interferograms from 6−8 different samples. Where necessary, small baseline drifts due to swelling/shrinkage of the protein were subtracted. The frequency positions of markings are identical to those in trace A unless otherwise labeled. For comparison, trace A (unlabeled, H_2O, gray) has been overlaid on the spectra of labeled materials.

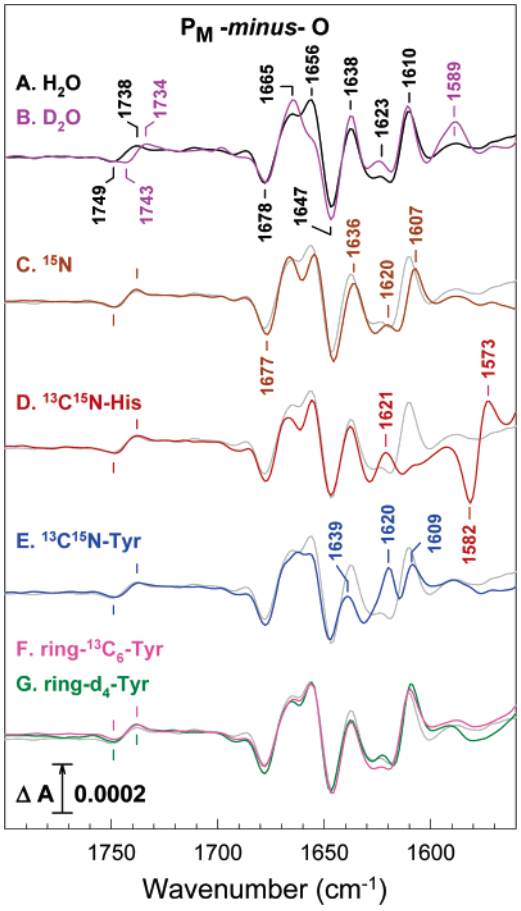

FIGURE 4: Isotope effects on the 1800−1560 cm^{-1} region of P_M *minus* O spectra. Spectra were recorded as described in Materials and Methods, with the transition generated by switching from an aerobic buffer at pH/D 9.0 containing 0.2 mM potassium ferricyanide to an identical one that had been briefly gassed with CO. All isotopically labeled enzymes were measured in H_2O media. Spectra are unlabeled in H_2O buffer (A, black) or in D_2O buffer (B, purple), universal ^{15}N-labeled (C, brown), $^{13}C_6{}^{15}N_3$-histidine-labeled (D, red), $^{13}C_9{}^{15}N$-tyrosine-labeled (E, blue), ring-$^{13}C_6$-tyrosine-labeled (F, pink), and ring-d_4-tyrosine-labeled (G, green) forms. Typically, spectra from 6−8 different samples were averaged, each of which was derived from 4000 averaged interferograms. Where necessary, small baseline drifts due to swelling/shrinkage of the protein were subtracted. The frequency positions of markings are identical to those in trace A unless otherwise labeled. For comparison, trace A (unlabeled, H_2O, gray) has been overlaid on the spectra of labeled materials.

the high (1800−1560 cm^{-1}), middle (1580−1260 cm^{-1}), and low (1280−900 cm^{-1}) frequency regions of these spectra are expanded and overlaid on unlabeled spectra in Figure 3, 5, and 7. Spectra of the unlabeled enzyme in H_2O and D_2O, universally ^{15}N-labeled and ring-d_4-tyrosine-labeled materials (traces A−C and G) are consistent with previously reported data on cytochrome oxidase from *P. denitrificans* (*28*, *32*, *41*, *48*, *60*) but have improved signal/noise and an extended spectral window. Similarities with spectra of related oxidases from other sources are also evident (*29*, *42*, *61*, *62*). Spectra D−F have not been reported previously. Comparisons of spectra allow improved assignments of bands to amide I/II backbone changes, cofactors, and specific amino acids, as detailed below and summarized in Table 1.

Amide I/II Changes. Spectra of proteins are typically dominated by amide I and II changes in the 1700−1600 and 1570−1500 cm^{-1} regions, respectively. The prominent 1660 cm^{-1} peak (Figure 3A) has been associated primarily with heme *a*, whereas the 1641 cm^{-1} trough and 1631 cm^{-1} peak have been associated with heme a_3 (*60*). As expected for amide I bands, only small changes are evident with H/D exchange (Figure 3A and B) or universal ^{15}N-labeling (Figure 3C), and no changes occur in ring-labeled tyrosine samples (Figure 3F and G). However, in samples in which the amide bond atoms of histidine (Figure 3D) or tyrosine (Figure 3E) are labeled, quite marked bandshifts are seen, demonstrating that the amide bonds of these residues have a significant contribution to the net amide I bandshifts. A similar bandshift, which resulted in the appearance of a 1604 cm^{-1} band, has been reported in the reduced *minus* oxidized spectrum of 1-^{13}C-Tyr-labeled *bo* type oxidase (*63*).

The 1580−1500 cm^{-1} amide II regions are shown in greater detail in Figure 5. Again, no significant effects of tyrosine ring labeling are seen (Figure 5F and G), although

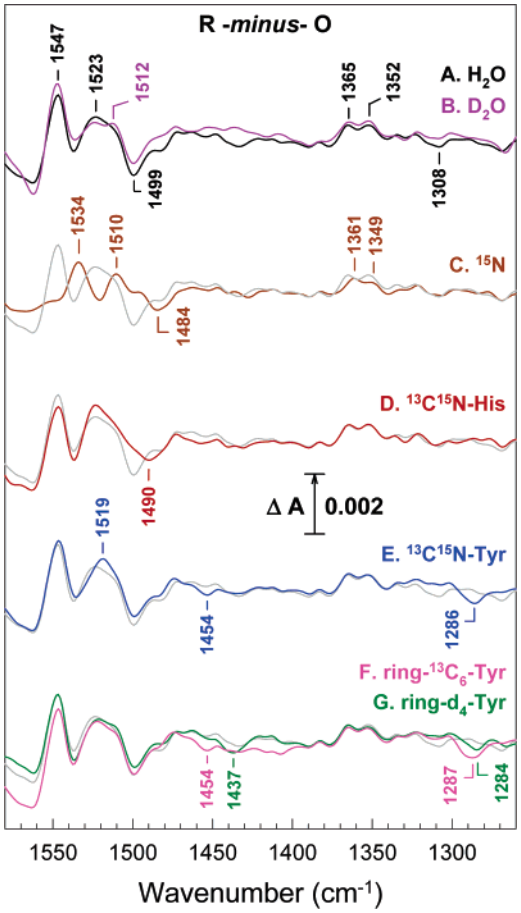

FIGURE 5: Isotope effects on the 1580−1260 cm^{-1} region of R *minus* O difference spectra. Experimental conditions, color codes, and alphabetical symbols are the same as those in Figure 3. For comparison, trace A (unlabeled, H_2O, gray) has been overlaid on the spectra of labeled materials.

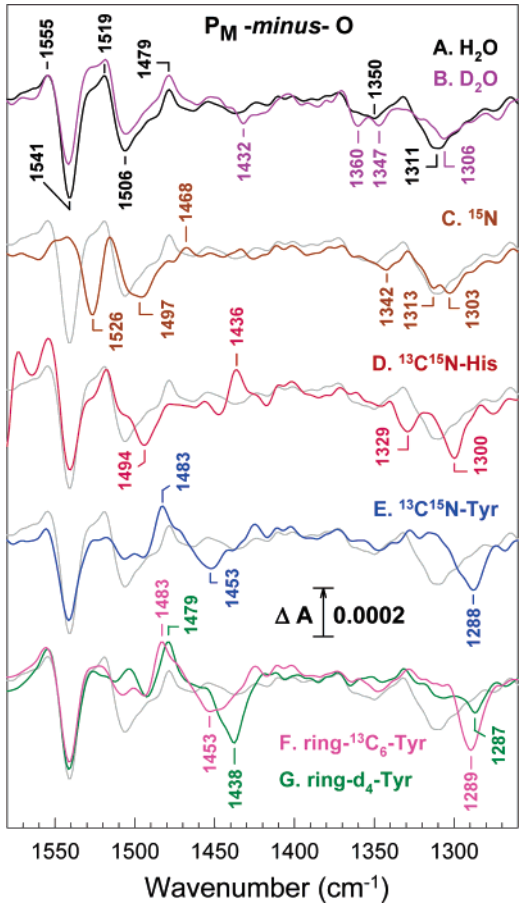

FIGURE 6: Isotope effects on the 1580−1260 cm^{-1} region of P_M *minus* O difference spectra. Experimental conditions, color codes, and alphabetical symbols are the same as those in Figure 4. For comparison, trace A (unlabeled, H_2O, gray) has been overlaid on the spectra of labeled materials.

some decreases are seen in materials with labeled tyrosine or histidine amide bonds (Figure 5D and E), consistent with the amide I effects above. Much more dramatic effects are observed with universal ^{15}N-labeling (Figure 5C), which could be consistent with a large amide II contribution to changes in this region. However, roughly half of the band intensity remains, and in contrast to amide II behavior, the effects of H/D exchange (Figure 5A and B) are relatively small. This indicates that the region is dominated by other major contributors such as hemes (see below).

Heme-Associated Bands. Heme prosthetic groups have a range of vibrational modes across the IR ranges studied here, and many of these are redox-dependent (*64*−*67*). Some good model heme A Raman data are available (*68*, *69*), although equivalent IR data of a heme A model compound have not yet been reported. In bovine oxidase, the formyl group of heme a_3 shifts from 1676 to 1661 cm^{-1} on reduction, the formyl group of heme *a* shifts from 1650 to 1620 cm^{-1}, and the vinyl groups of the reduced hemes have a positive C═C vibration at 1616−7 cm^{-1} (*35*, *65*, *66*, *69*−*71*). Such shifts must contribute to the amide I region but are obscured by the larger amide I changes. It seems likely that shifts of C═O stretches of protonated heme propionic acid(s) will also contribute around 1700−1680 cm^{-1} because at least one of the four has been suggested to be protonated at pH 7 with a band at 1676 cm^{-1} (*33*). The positive bands at 1696 and 1683 cm^{-1} are both candidates because of their H/D sensitivity.

As noted above, it is clear that the 1580−1500 cm^{-1} region has major nonamide II contributions. Strong redox-dependent bands of heme appear in this region (*67*), and Raman data indicate that their ^{15}N-induced downshifts are less than 2 cm^{-1} (*72*). Combining this with the observed isotope effects seen in Figure 5, it is evident that heme bands are major contributors to this region. Indeed, Gorbikova et al. (*60*) have assigned the two major positives labeled as 1547 and 1523 cm^{-1} mainly to reduced hemes *a* and a_3, respectively. A range of other redox-sensitive heme ring IR bands can occur (*42*, *64*−*69*, *71*), and the clearest of these are the ^{15}N-sensitive positive bands at 1365 and 1352 cm^{-1}.

Specific Amino Acids. Protonated carboxylic acids absorb strongly in the 1750−1700 cm^{-1} region (*54*). The R *minus* O spectrum of the unlabeled enzyme exhibits a change at 1747/1738 cm^{-1} (Figure 3A and (*28*, *32*, *42*, *48*, *60*, *71*)), which appears from its symmetry to arise from perturbation of a single group. Work from several laboratories with mutant forms of bacterial oxidases has shown clearly that features in this region arise predominantly from the protonated form of the equivalent of Glu278 (*28*, *31*, *62*, *73*, *74*). The 5 cm^{-1} downshift on H/D exchange and insensitivity to all other labeling (Figure 3B) further confirms its carboxylic acid origin (*32*, *39*, *41*, *75*). The same region of the equivalent IR difference spectrum of bovine oxidase has bands that must

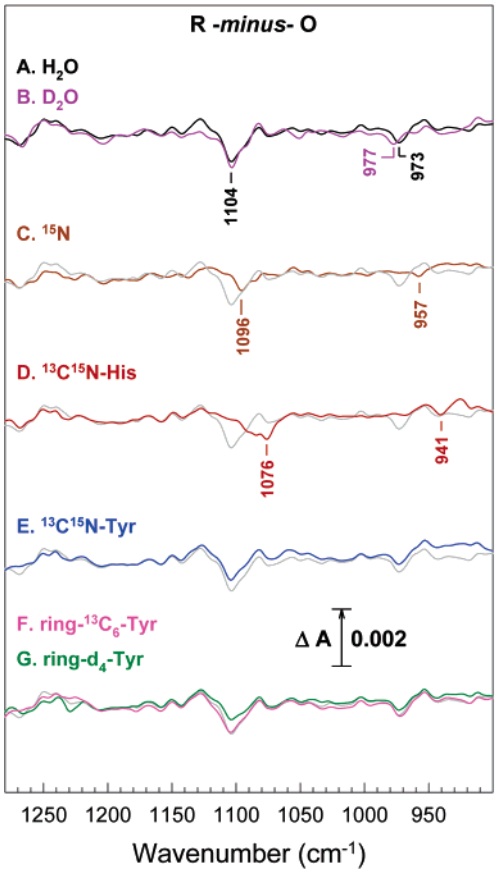

FIGURE 7: Isotope effects on the 1280−900 cm^{-1} region of R *minus* O difference spectra. Experimental conditions, color codes, and alphabetical symbols are the same as those in Figure 3. For comparison, trace A (unlabeled, H_2O, gray) has been overlaid on the spectra of labeled materials.

arise from the perturbation of at least two carboxylic acid groups (*32*, *71*, *75*), and it is possible that the redox-linked carboxylic region of the *P. denitrificans* oxidase also reflects change of more than one residue (*28*).

Any shifts of the 1518 cm^{-1} υ(CC) band of tyrosines in the R *minus* O spectra of Figure 5 are masked by the much stronger amide II band changes. However, the troughs at 1454 cm^{-1} in ring-^{13}C-labeled (Figure 5E and F) and at 1437 cm^{-1} in ring-d_4-labeled (Figure 5G) proteins should arise from the same downshifted tyrosine band (cf. Figure 1). A further tyrosine signature is that arising from the υ(CO), υ(CC) band (*41*, *54*, *55*), which appears at 1284−1287 cm^{-1} in the tyrosine ring-labeled samples (Figure 5E−G), perhaps arising from a downshift of the 1308 cm^{-1} trough seen in the unlabeled material (Figure 5A).

Bands arising from ring C−N bonds of the histidine headgroup are expected in the 1100−1900 cm^{-1} range (*54*, *57*−*59*) and Figure 7), a region free of other major amino acid contributions. Troughs at 1104 and 973 cm^{-1} in the unlabeled enzyme (Figure 7A) were downshifted by both universal ^{15}N and $^{13}C_6{}^{15}N_3$-histidine labeling (Figure 7C and D) but were insensitive to the labeling of tyrosine (Figure 7E−F). Hence, definitive assignment of both bands to histidine changes can be made. A similar downshift of the 1104 cm^{-1} band was reported recently in equivalent redox difference spectra of oxidase from *Rhodobacter sphaeroides* with universal ^{15}N and ^{15}N-histidine labeling (*42*). This frequency is within the 1103−1112 cm^{-1} range found for the C5N1 bond of neutral histidine bound by its N_τ to a metal (*58*). Gorbikova et al. (*60*) have recently associated the 1104 cm^{-1} trough, together with a peak at 1128 cm^{-1}, with histidine ligands of oxidized Cu_B. In addition, however, histidine-ligated hemes usually have strong negative bands at this position in reduced *minus* oxidized difference spectra (*67*, *76*, *77*). Hence, it may be concluded that the bands arise predominantly from perturbation of one or more of the histidine ligands to Cu_B and/or hemes *a* and a_3.

P_M Minus O IR Difference Spectra

An overview of the P_M *minus* O IR difference spectra of unlabeled and labeled proteins is given in Supporting Information (Figure S2). For ease of comparison, the high (1800−1560 cm^{-1}), middle (1580−1260 cm^{-1}), and low (1290−1950 cm^{-1}) frequency regions of these spectra are expanded and overlaid on unlabeled spectra in Figures 4, 6, and 8. Spectra of unlabeled enzyme in H_2O and D_2O, universal ^{15}N-labeled and ring-d_4-tyrosine-labeled materials (traces A−C and G) are consistent with previously reported data on P_M in cytochrome *c* oxidase from *P. denitrificans* (*39*, *40*, *48*) but have improved signal/noise and an extended spectral window. Spectra D−F have not been reported previously. Again, comparisons of spectra allow improved assignments of bands to amide I and II backbone changes, cofactors, and specific amino acids (summarized in Table 1).

Amide I/II Changes. The 1800−1560 cm^{-1} regions are shown in greater detail in Figure 4. Again as expected for amide I bands, 2−3 cm^{-1} downshifts are evident with universal ^{15}N-labeling (Figure 4C), and no significant changes occur in ring-labeled tyrosine samples (Figure F and G). H/D exchange did, however, cause a more significant change than that expected for amide I effects with the loss of the 1656 cm^{-1} peak and the appearance of a new positive at 1589 cm^{-1} (Figure 4B), and these are assigned (see below) to an arginine perturbation. Of particular note, however, were prominent bandshifts in samples in which the amide bond atoms of histidine (Figure 4D) or tyrosine (Figure 4E) were labeled (cf. amide I band downshifts caused by $^{13}C^{15}N$-labeling in (*78*, *79*)). Specifically, $^{13}C_6{}^{15}N_3$- labeling of the amide bonds of histidine caused a bandshift with a peak at 1610 cm^{-1} in unlabeled material to appear instead as a peak/trough at 1573/1582 cm^{-1}. $^{13}C_9{}^{15}N$-labeling of the amide bonds of tyrosine caused a bandshift that had a peak at 1638 cm^{-1} in unlabeled material to appear instead as a peak at 1620 cm^{-1}. The two bands make a significant contribution to the total amide I changes, suggesting that amide I bonds of both histidine and tyrosine residues are major components of a conformational change that is associated with the P_M state.

The tyrosine-specific 1638 cm^{-1} band is within the expected range for β secondary structure. An equivalent band was observed in bovine oxidase at 1637 cm^{-1} and appeared to persist in the F state (*39*). However, the histidine-specific 1610 cm^{-1} band is at the very limit of the usual amide I frequency range (*80*). Its unusually low frequency may arise from the strained backbone structure of Tyr280−His276−Pro277, where besides the covalent His−Tyr bond, the amide carbonyl of His276 is directly bonded to the ring N-H of Pro277 and is also close to the backbones of Glu278 and

Table 1: Summary of Bands and Their Assignments[a]

reduced *minus* oxidized		P_M *minus* oxidized	
frequency (cm^{-1})	comments	frequency (cm^{-1})	comments
	Amide I/II Bands		
1696(+),1683(+)	possible propionic acid contributions	1678(−)/1665(+)	amide I (+heme a_3 formyl)
1670(−)		1656(+)	amide I (+Arg)
1660(+)	in part, Tyr and His amide I; associated with heme *a* redox change	1647(−)	
1641(−)/1631(+)	associated with heme a_3 redox change	1638(+)	Tyr amide I
1617(+)	Tyr amide I	1623(+)	
		1610(+)	His amide I
	Heme		
1696(+)	heme propionic acid	1678 (−)/1665(+)	heme a_3 formyl (+amide I)
1547 (+)	ferrous heme *a* ring		
1523 (+)	ferrous heme a_3 ring	1541(−)	possibly heme a_3 (formerly assigned to C−N bond in His−Tyr)
1365 (+)	heme ring	1479(+)	ferryl heme a_3
1352 (+)	heme ring	1233(+)	ferryl heme a_3
	redox-dependent bandshifts due to a_3 formyl (1661(+)/1676(−)), *a* formyl (1620(+)/1620(−) and vinyl (1616(+)) substituents should also be present but are obscured by larger amide I bands.		other weak heme bands in the 1400 and 1350 regions are probable, but are overlapped by other components.
	Amino Acids		
1747(−)/1738(+)	ν(C═O) Glu (Glu278)	1749(−)/1738(+)	ν(C═O) Glu (Glu278)
1455(−) *or* 1435(−)	υ(CC) at 1455 cm^{-1} in ring-^{13}C-labeled and at 1435 cm^{-1} in ring-d_4-labeled Tyr (unlabeled tyrosine band at 1518 obscured by other bands)	1656(+)	ν guanidinium of Arg, probably Arg473 or Arg474. Most clearly seen at 1589(+) in D_2O
1284−7	υ(CO), υ(CC) in ring-^{13}C-labeled and ring-d_4-labeled Tyr (unlabeled Tyr band uncertain)	1519(+)	His−Tyr, possibly neutral phenolic radical ring
1128(+)	metal-ligated His	1506(−)	His−Tyr
1104(−)	C5N1 of His, most likely neutral, N_τ-metal-ligated	1311(−)	His−Tyr
973(−)	His ring	1129(+)	His−Tyr
		1094(−)	His−Tyr
		1106(+)/1082(−)	His, possibly proximal ligand of heme a_3

[a] Detailed reasons for assignments and relevant literature are provided in the text.

Val279. Bovine P_M *minus* O spectra also have an equivalent band at 1611 cm^{-1}, which in this case does not persist in the F state (*39*). This suggests that further analyses of these bands in different intermediates may reveal more precise details of conformational changes at the active site.

The 1580−1500 cm^{-1} regions are shown in greater detail in Figure 6. As reported previously (*39*, *48*), the dominating trough at 1541 cm^{-1} was only partially diminished by H/D exchange (Figure 6A and B), but was downshifted to 1526 cm^{-1} by universal ^{15}N-labeling (Figure 6C). In addition, no significant effects on this band were observed in any of the tyrosine- or histidine-labeled materials. Although the 15 cm^{-1} downshift with universal ^{15}N-labeling would be consistent with a significant amide II origin, the partial decrease with H/D exchange (despite further attempts to maximize the extent of H/D exchange) is not consistent with a wholly amide II origin unless the site is particularly resistant to exchange. As a result, we had suggested (*39*) on the basis of related model compound data (*56*, *81*−*86*) that the band might arise from the covalent C−N bond link of the protonated form of the His−Tyr dimer. However, the absence of effects of labeling of the rings of histidine or tyrosine (Figure 6D−G) must call this assignment into question. An alternative possible heme origin of this band is explored below, as are the clear tyrosine contributions to the shifts around 1500 cm^{-1} that are revealed by labeling of the tyrosine ring (Figure 6E−G).

Heme-Associated Bands. Contributions of heme a_3 are to be expected and it is likely that the 1678 cm^{-1} trough that is seen consistently in all P_M *minus* O spectra in Figure 4 arises from the heme a_3 formyl group (*35*, *69*−*71*), possibly shifting to 1665 cm^{-1} in a ferric to ferryl conversion. The heme A

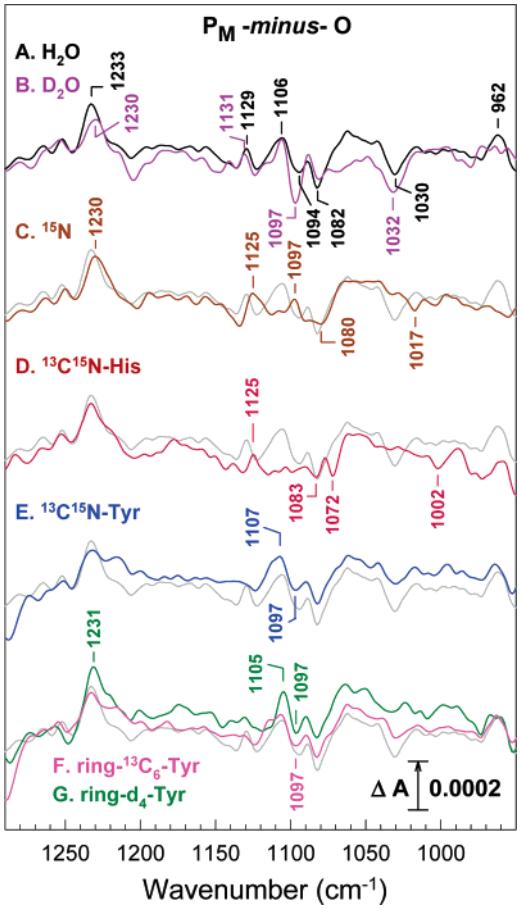

FIGURE 8: Isotope effects on the 1290−950 cm^{-1} region of P_M *minus* O difference spectra. Experimental conditions, color codes, and alphabetical symbols are the same as those in Figure 4. For comparison, trace A (unlabeled, H_2O, gray) has been overlaid on the spectra of labeled materials.

vinyl group can also have a strong positive band in the 1620−1600 cm^{-1} region, at least in the ferrous heme state (*70*, *71*). However, the 3 cm^{-1} downshift with universal ^{15}N-labeling (Figure 4C) and the shift to 1573 cm^{-1} with labeled histidine (Figure 4B) confirm that this band in the P_M *minus* O spectra is predominantly an amide I shift.

We have previously suggested that the sharp H/D-insensitive band at 1479 cm^{-1} might arise from ferryl heme a_3 (*39*, *48*), although an assignment to a tyrosine radical has also been suggested (see below). The persistence of this band in the tyrosine-labeled samples and its sensitivity to universal ^{15}N-labeling suggests that the ferryl heme assignment may still be valid, though it is not possible to assess whether it remains in the labeled histidine spectrum because of overlapping bands.

In ferrous *minus* ferric model heme B spectra, redox-sensitive IR bands can occur in the 1550−1500, 1410, 1330, 1230, and 1120 cm^{-1} regions (*64*−*69*) though, unfortunately, IR data on model ferryl heme B compounds data are not available. In the P_M *minus* O spectra, the positive, ^{15}N-labeling-sensitive band at 1233 cm^{-1} (Figure 8A) most likely arises from ferryl heme a_3, as might some of the changes occurring around 1400 and 1350 cm^{-1}, although these latter regions have multiple weak overlapping components that prevent specific assignments. In addition, given the ^{15}N-sensitivity of the large trough at 1541 cm^{-1} and its lack of sensitivity H/D exchange and to histidine and tyrosine labeling, the possibility that a large part arises from a ferric heme a_3 band seems likely.

Bands Attributable to Covalent His−Tyr in O-State Oxidase. A particularly topical question on the chemistry of P_M concerns the role in the catalytic mechanism of the unusual covalently linked His−Tyr ligand to Cu_B (*23*, *87*, *88*), with the consensus expectation that this acts as a proton and electron donor and forms a neutral radical in P_M that is re-reduced and possibly reprotonated to form the subsequent F intermediate. However, no EPR signature could be found, possibly because of spin coupling with the paramagnetic Cu_B^{2+} (*26*, *89*), and other spectroscopies such as IR are necessary. Useful comparisons can be made with IR and Raman data on model materials that are related to tyrosine and His−Tyr (*56*, *81*−*85*), with tyrosine radical/tyrosine-OH IR difference spectra that can be generated in photosystem II (*55*) and with the model IR spectra of the labeled tyrosines and histidine (Figures 1 and 2). The spectra presented here provide the opportunity for definitive identification of some of the bands associated with this dimer that are sensitive to isotope labeling of both tyrosine and histidine headgroups.

The formation of a neutral radical in P_M should result in negative bands due to loss of the ground state. Tomson et al. (*81*) reported a band at 1546 cm^{-1} in D_2O for a model compound that was suggested to be uniquely associated with the ground state His−Tyr C−N linkage. A corresponding band at 1549 cm^{-1} in photolyzed CO-ligated cytochrome bo_3, together with two others at 1483 and 1412 cm^{-1}, was downshifted with ^{15}N-labeling. In the same report, some rather weaker evidence was presented that ring-d_4-tyrosine labeling also caused a similar downshift in the 1549 but not the 1483 and 1412 cm^{-1} bands. Hellwig et al. (*41*) reported prominent bands at 1547 and 1345 cm^{-1} in a related model material in H_2O, which were lost when the phenolic group became deprotonated. When the radical state was generated from the deprotonated form of a further related model compound, a band at 1303 cm^{-1} was lost (*82*), although clear positive bands that might be assigned to the radical were not evident.

On the basis of such model compound data, we have suggested previously that the 1541−7 and 1311−4 cm^{-1} troughs in the P_M *minus* O IR difference spectra could be assigned to the deprotonation of the phenolic group of the His−Tyr when going from the oxidized to the P_M state (*48*). The data in Figure 6 extend this analysis. Upon universal ^{15}N-labeling (Figure 6C), the trough at 1541 cm^{-1} was downshifted by 15 cm^{-1}, consistent with data in (*81*) and showing that it is associated with a nitrogenous element. However, traces D−G in Figure 6 show little or no decreases in its amplitude or frequency on labeling of the headgroups of tyrosine or histidine. Data in ref 81 suggest that ring-d_4-tyrosine labeling should downshift the 1542 cm^{-1} band by 9−13 cm^{-1}. Labeling of free tyrosine-OH results in loss of the 1518 cm^{-1} υ(C−C) band and the appearance of a new band at 1414 cm^{-1} (ring-d_4-labeled) or 1481 cm^{-1} (ring-$^{13}C_6$-labeled) (Figure 1). Similarly, in $Y_D^{\bullet}/Y_DOH$ difference spectra of photosystem II ring-d_4 labeling results in the replacement of a trough around 1490 cm^{-1} with one at 1428 cm^{-1} (*90*). In the P_M *minus* O spectra of Figure 6, ring labeling of tyrosine caused a loss of the 1506 cm^{-1} trough, together with a prominent new trough at 1453 cm^{-1} (ring-$^{13}C_6$; Figure 6E and F) or 1438 cm^{-1} (ring-d_4; Figure 6G).

However, universal ^{15}N and histidine labeling also caused a downshift of the band by approximately 10 cm^{-1}. Hence, although the new data here cannot support the previously suggested His−Tyr bond origin of the major part of the 1541 cm^{-1} trough in P_M *minus* O spectra, it is clear that a major part of the 1506 cm^{-1} trough is from this structure. This also appears to be true for the 1311 cm^{-1} trough (*48*) because this was also downshifted −22 to −24 cm^{-1} with labeled tyrosines (Figure 6E−G) or −11 cm^{-1} with labeled histidine (Figure 6D).

The P_M *minus* O spectra also have peaks at 1129 and 1106 cm^{-1} and troughs at 1094 and 1082 cm^{-1} (Figure 8A). Shifts with H/D exchange (Figure 8B), universal ^{15}N (Figure 8C) and $^{13}C_6{}^{15}N_3$-histidine labeling (Figure 8D) are consistent with a histidine origin (Figure 3 and (*54*, *57*−*59*)). In addition, however, the 1129 cm^{-1} peak is lost, and the 1094 cm^{-1} trough is upshifted by 3 cm^{-1} with ring labeling of tyrosine (Figure 8E−G), suggesting that these bands arise from the covalently linked histidine, whereas the 1082 cm^{-1} trough should arise from another histidine, most likely the proximal histidine that is ligated to heme a_3 and responding to its redox state change.

In summary, the new data support assignment of the 1506, 1311, and 1094 cm^{-1} troughs and the 1129 cm^{-1} peak in P_M *minus* O difference spectra to the ground state His−Tyr structure but do not support the same assignment of the trough at 1541−1547 cm^{-1}, although such a band is seen in protonated His−Tyr model compounds. Nevertheless, the data show definitively that this dimer is undergoing a significant change in the O to P_M transition. A key issue in relation to this is its protonation and redox state throughout the steps in the catalytic cycle. On the basis of model compound spectra and comparisons with $Y_D^{\bullet}/Y_DOH$ difference spectra, we have previously favored the view that the tyrosine hydroxyl group is protonated in the O state. Unfortunately, the present data cannot provide a definitive answer on this point. Ring labeling shifts the frequency of the two principal tyrosine bands near 1500 and 1250 cm^{-1} in a similar manner for both tyrosine protonation states, but the effects on extinction coefficients are dramatically different (Figure 1). Although the His−Tyr dimer will have vibrational properties quite distinct from those of free tyrosine, it may be noted that the troughs at 1311 and 1506 cm^{-1} in the P_M *minus* O spectra exhibit a pattern of intensity changes on ring-labeling that is closer to that seen in the tyrosinate, rather than the tyrosine, model data of Figure 1. On this basis, the data would favor the tyrosine being deprotonated in the O state. As a result, current results cannot provide a definitive assignment on this important point, and further work on labeling, models and calculations will be required to settle the point.

Bands Attributable to Covalent His−Tyr in the P_M State. IR and Raman features of neutral phenoxyl radical models and tyrosine radicals in photosystem II and other proteins (*55*) show two prominent modes of the neutral phenolic radical, υ(C−C) at 1550−1610 cm^{-1} and υ_{7a}(C-O) at 1480−1530 cm^{-1}. Equivalent bands should occur in the His−Tyr radical, though a Raman study (*83*) has emphasized the importance of the relative orientations of the phenolic and imidazole rings in governing the vibrational spectra of such compounds, and the covalent linkage of the tyrosine to a metal-bound histidine may further distort such a comparison. A Raman band at 1489 cm^{-1} identified in the P_M state of bacterial cytochrome bo_3 was tentatively assigned to a tyrosine radical rather than to heme (*24*). In addition, Nyquist et al. (*40*) suggested that a 1479 cm^{-1} band in their P_M *minus* O IR difference spectra of cytochrome *c* oxidase from *R. sphaeroides* might arise from a tyrosine radical (together with bands at 1587, 1528, and 1517 cm^{-1}; see below). However, in a previous study, we observed that the 1480 cm^{-1} peak persisted in the F state (albeit at lower intensity in the *Paracoccus* enzyme), a state in which a radical should not occur (*39*). The spectra of labeled proteins, although overlapping with other changes is a problem in this region, also tend to rule out such an origin, particularly because it is affected by universal ^{15}N (Figure 6C) and, apparently, histidine labeling (Figure 6D), and instead support a ferryl heme a_3 (or its proximal histidine ligand) origin. Likewise, most of the band seen near 1590 cm^{-1} ((*40*) and Figure 4) does not appear to be associated with the His−Tyr dimer because it is hardly affected by universal ^{15}N (Figure 4C) or tyrosine ring labeling (Figure 4E−G).

We have previously argued that a positive band at 1519 cm^{-1} and, with less confidence, a smaller peak at around 1570 cm^{-1} in the P_M *minus* O spectra might be the two expected bands of a neutral phenolic radical because they were unaffected by H/D exchange and did not persist in F (*39*). The 1519 cm^{-1} band is relatively unaffected by universal ^{15}N labeling (Figure 6C) or $^{13}C_6{}^{15}N_3$-histidine labeling (Figure 6D) but is shifted down to 1479−1483 cm^{-1} in labeled tyrosine samples (Figure 6E−G). The 1570 cm^{-1} band is too weak to ascertain its behavior with confidence. Hence, the 1519 cm^{-1} band, which is not seen in the F state (*39*, *40*), does indeed appear to be associated with the His−Tyr dimer, probably representing one of the bands of a neutral phenolic radical state in P_M.

Bands Attributable to Additional Amino Acids. Although the tyrosine and histidine changes described above appear to be mainly associated with the covalent His−Tyr dimer, it is possible that other nearby tyrosine and histidine residues appear in the spectra. In particular, the complex shape of P_M *minus* O spectra in the region around 1100 cm^{-1} (Figure 8), where C−N stretching modes of histidine side chains are expected indicates multiple species, with the 1082 cm^{-1} trough most likely arising from the proximal histidine of heme a_3.

A further feature in the P_M *minus* O data that warrants comment is the appearance in the H/D spectrum of a peak at 1589 cm^{-1}, together with a loss of intensity around 1656 cm^{-1} (Figure 4B). This change is not observed in any of the other spectra. From available data on major bands of different amino acids, the only possible candidate for this effect is from arginine, where the ν_{as} and ν_s bands of the guanidinium headgroup in solution shift from 1672−1673 and 1633−1636 cm^{-1} in the protonated form to 1608 and 1586 cm^{-1} when deuterated (*54*, *91*). Model arginine data (not shown) indicate only a 14 cm^{-1} downshift of the ν_{as} band of the guanidinium band with ^{15}N-labeling, again consistent with effects seen (Figure 4C). The most obvious candidates for the residue concerned are the conserved arginines, Arg473 or Arg474, which form ion pairs with the heme a_3 propionates (*1*, *33*). Of these, Arg473 may be the more likely one because it interacts strongly with the Δ-propionate of heme a_3, whereas Arg474 interacts with the propionate of heme *a*.

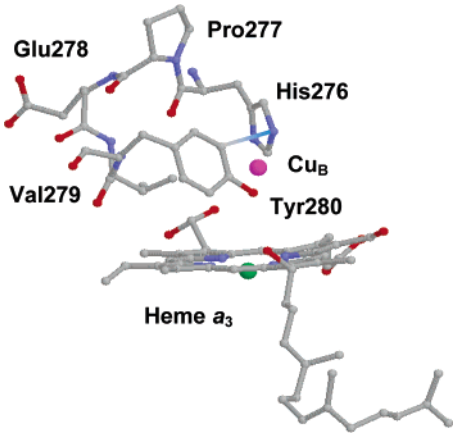

FIGURE 9: Structure of the HPEVY region and heme a_3/Cu_B. The diagram was extracted from the coordinates in PDB file 1AR1 of oxidized cytochrome *c* oxidase of *P. denitrificans* (*21*). Residues His276−Pro277−Glu278−Val279−Tyr280 have been oriented to highlight the covalent bond between the ortho carbon of Tyr280 and the N_τ nitrogen of His276.

Changes in the 1740 cm^{-1} carboxylic acid region in P_M that relax in F have been observed previously (*39*, *40*). In the *R. sphaeroides* oxidase, they appeared as a trough with no clear associated peak and were interpreted in terms of glutamic acid deprotonation in P_M (*40*). Recent IR studies of a homologous oxidase in which a tyrosine residue substitutes functionally for the glutamic acid and appears to deprotonate in P_M (*92*) have been taken to corroborate this view. In the case of bovine and *P. denitrificans* oxidases ((*39*) and Figure 4), however, a relatively symmetrical 1749/1738 cm^{-1} trough/peak occurs. Its downshift with H/D exchange (Figure 4B) and its insensitivity to universal ^{15}N or tyrosine or histidine labeling (Figure 4C−G) are also consistent with a carboxylic acid origin. Because of its clear peak/trough shape in these spectra, we continue to assign it to an environmental shift of a protonated carboxylic acid rather than to a protonation change. The differences with data in (*40*) could mean that the pK of the glutamic acid in the P_M form is below 8.5 in *R. sphaeroides*, whereas it is clearly above 9 in the *P. denitrificans* and bovine heart enzymes. Assignment to glutamic acid Glu278 remains most likely on the basis of mutagenesis data (*28*, *31*, *62*, *73*, *74*), with the change associated with its central role in providing a pathway for intraprotein proton transfer for both proton translocation and, as now seems likely, substrate proton delivery to the oxygen reduction site (*93*−*98*). The simplest explanation for the downshift of the band is in terms of a stronger hydrogen bonding of the COOH group in the P_M state. This might arise from a reorientation of the group itself, or from movement of water molecules in the cavity around the P_M state of the binuclear center that are thought to reorient during catalysis in order to facilitate correct proton-transfer pathways (*96*).

Combining the changes at the Glu278 headgroup with the evidence that backbones of both histidine and tyrosine contribute strongly to the amide I shifts in the P_M *minus* O spectra (Figure 4), it may be proposed that a conformational change occurs in P_M that involves the pentameric His276−Pro277−Glu278−Val279−Tyr280 (HPEVY) structure that is formed because of the covalent link between His276 and Tyr280 (Figure 9), with amide I backbone changes of the pentamer mediating the conformational change induced in the glutamic acid headgroup of the same pentamer and resulting in the observed 1749/1738 cm^{-1} shift. The conformational changes will likely affect other amino acid headgroups in this pentamer and its surrounding residues and might be the primary cause of many of the other headgroup bandshifts described here. It might be noted that a similar carboxylic shift is also observed in the R *minus* O difference spectra (Figure 3), although the much more extensive amide I changes obscure whether the same HPEVY backbone changes are occurring. It does, however, appear that the environmental change that affects the side chain of Glu278 is not unique to the P_M state but also occurs already on reduction of the enzyme, possibly prior to its reaction with O_2 to form P_M. Such structural changes are critically required throughout the catalytic cycle in order to ensure the making and breaking of proton-transfer pathways for correctly orchestrated movements of substrate and translocated protons, and it is quite likely that many will be too subtle to be discernible from X-ray analyses. Extension of the IR analyses here to time-resolved identification of structural changes in additional catalytic steps would provide the bridge between the static crystal structures and the atomic details of the dynamic mechanism of coupled proton/electron transfers.

ACKNOWLEDGMENT

We are grateful to Mr. Santiago Garcia for specialist electronic and mechanical support and Ms. Eija Haasanen, Anne Hakonen, and Tarja Salojärvi for excellent help in producing the auxotroph and with bacterial culturing.

SUPPORTING INFORMATION AVAILABLE

Collated ATR-FTIR spectra of R *minus* O (1800−1900 cm^{-1}) and P_M *minus* O (1800−1950 cm^{-1}) difference spectra over the entire frequency range. This material is available free of charge via the Internet at http://pubs.acs.org.

REFERENCES

1. Iwata, S., Ostermeier, C., Ludwig, B., and Michel, H. (1995) Structure at 2.8 Å resolution of cytochrome *c* oxidase from *Paracoccus denitrificans*, *Nature 376*, 660−669.
2. Tsukihara, T., Aoyama, H., Yamashita, E., Tomizaki, T., Yamaguchi, H., Shinzawa-Itoh, K., Nakashima, R., Yaono, R., and Yoshikawa, S. (1996) The whole structure of the 13-subunit oxidized cytochrome *c* oxidase at 2.8 Å, *Science 272*, 1136−1144.
3. Svensson-Ek, M., Abramson, J., Larsson, G., Törnroth, S., Brzezinski, P., and Iwata, S. (2002) The X-ray crystal structures of wild-type and EQ(I-286) mutant cytochrome *c* oxidases from *Rhodobacter sphaeroides*, *J. Mol. Biol. 321*, 329−339.
4. Morgan, J. E., Verkhovsky, M. I., and Wikström, M. (1996) Observation and assignment of peroxy and ferryl intermediates in the reduction of dioxygen to water by cytochrome *c* oxidase, *Biochemistry 35*, 12235−12240.
5. Sucheta, A., Georgiadis, K. E., and Einarsdóttir, O. (1997) Mechanism of cytochrome *c* oxidase-catalysed reduction of dioxygen to water: evidence for peroxy and ferryl intermediates at room temperature, *Biochemistry 36*, 554−565.
6. Nicholls, P., and Chanady, G. A. (1981) Interactions of cytochrome aa_3 with oxygen and carbon monoxide. The role of the 607 nm complexes, *Biochim. Biophys. Acta 634*, 256−265.
7. Ädelroth, P., Ek, M., and Brzezinski, P. (1998) Factors determining electron-transfer rates in cytochrome *c* oxidase: investigation of the oxygen reaction in the *R. sphaeroides* enzyme, *Biochim. Biophys. Acta 1367*, 107−117.
8. Sucheta, A., Szundi, I., and Einarsdóttir, O. (1998) Intermediates in the reaction of fully reduced cytochrome *c* oxidase with dioxygen, *Biochemistry 37*, 17905−17914.

9. Karpefors, M., Ädelroth, P., Namslauer, A., Zhen, Y., and Brzezinski, P. (2000) Formation of the "peroxy" intermediate in cytochrome *c* oxidase is associated with internal proton/hydrogen transfer, *Biochemistry 39*, 14664−14669.
10. Morgan, J. E., Verkhovsky, M. I., Palmer, G., and Wikström, M. (2001) The role of the P_R intermediate of cytochrome *c* oxidase with O_2, *Biochemistry 40*, 6882−6892.
11. Wrigglesworth, J. M. (1984) Formation and reduction of a 'peroxy' intermediate of cytochrome *c* oxidase by hydrogen peroxide, *Biochem. J. 217*, 715−719.
12. Fabian, M., and Palmer, G. (1995) The interaction of cytochrome oxidase with hydrogen peroxide: The relationship of compounds P and F, *Biochemistry 34*, 13802−13810.
13. Jünemann, S., Heathcote, P., and Rich, P. R. (2000) The reactions of hydrogen peroxide with bovine cytochrome *c* oxidase, *Biochim. Biophys. Acta 1456*, 56−66.
14. Proshlyakov, D. A., Pressler, M. A., and Babcock, G. T. (1998) Dioxygen activation and bond cleavage by mixed-valence cytochrome *c* oxidase, *Proc. Natl. Acad. Sci. U.S.A. 95*, 8020−8025.
15. Fabian, M., and Palmer, G. (1999) Redox state of peroxy and ferryl intermediates in cytochrome *c* oxidase catalysis, *Biochemistry 38*, 6270−6275.
16. Proshlyakov, D. A., Ogura, T., Shinzawa-Itoh, K., Yoshikawa, S., Appelman, E. H., and Kitagawa, T. (1994) Selective resonance Raman observation of the "607 nm" form generated in the reaction of oxidized cytochrome *c* oxidase with hydrogen peroxide, *J. Biol. Chem. 269*, 29385−29388.
17. Proshlyakov, D. A., Ogura, T., Shinzawa-Itoh, K., Yoshikawa, S., and Kitagawa, T. (1996) Microcirculating system for simultaneous determination of Raman and absorption spectra of enzymatic reaction intermediates and its application to the reaction of cytochrome *c* oxidase with hydrogen peroxide, *Biochemistry 35*, 76−82.
18. Proshlyakov, D. A., Ogura, T., Shinzawa-Itoh, K., Yoshikawa, S., and Kitagawa, T. (1996) Resonance Raman/absorption characterization of the oxo intermediates of cytochrome *c* oxidase generated in its reaction with hydrogen peroxide: pH and H_2O_2 concentration dependence, *Biochemistry 35*, 8580−8586.
19. Fabian, M., Wong, W. W., Gennis, R. B., and Palmer, G. (1999) Mass spectrometric determination of dioxygen bond splitting in the "peroxy" intermediate of cytochrome *c* oxidase, *Proc. Natl. Acad. Sci. U.S.A. 96*, 13114−13117.
20. Proshlyakov, D. A., Pressler, M. A., DeMaso, C., Leykam, J. F., DeWitt, D. L., and Babcock, G. T. (2000) Oxygen activation and reduction in respiration: Involvement of redox-active tyrosine 244, *Science 290*, 1588−1591.
21. Ostermeier, C., Harrenga, A., Ermler, U., and Michel, H. (1997) Structure at 2.7 Å resolution of the *Paracoccus denitrificans* two-subunit cytochrome *c* oxidase complexed with an antibody F_v fragment, *Proc. Natl. Acad. Sci. U.S.A. 94*, 10547−10553.
22. Mitchell, D. M., Ädelroth, P., Hosler, J. P., Fetter, J. R., Brzezinski, P., Pressler, M. A., Aasa, R., Malmström, B. G., Albeni, J. O., Babcock, G. T., Gennis, R. B., and Ferguson-Miller, S. (1996) A ligand-exchange mechanism of proton pumping involving tyrosine-422 of subunit I of cytochrome oxidase is ruled out, *Biochemistry 35*, 824−828.
23. Michel, H. (1999) Proton pumping by cytochrome *c* oxidase, *Nature 402*, 602−603.
24. Uchida, T., Mogi, T., and Kitagawa, T. (2000) Resonance Raman studies of oxo intermediates in the reaction of pulsed cytochrome *bo* with hydrogen peroxide, *Biochemistry 39*, 6669−6678.
25. Rigby, S. E. J., Jünemann, S., Rich, P. R., and Heathcote, P. (2000) The reaction of hydrogen peroxide with bovine cytochrome *c* oxidase produces a tryptophan cation radical and a porphyrin cation radical, *Biochemistry 39*, 5921−5928.
26. Rich, P. R., Rigby, S. E. J., and Heathcote, P. (2002) Radicals associated with the catalytic intermediates of bovine cytochrome *c* oxidase, *Biochim. Biophys. Acta 1554*, 137−146.
27. Hellwig, P., Rost, B., Kaiser, U., Ostermeier, C., Michel, H., and Mäntele, W. (1996) Carboxyl group protonation upon reduction of the *Paracoccus denitrificans* cytochrome *c* oxidase: Direct evidence by FTIR spectroscopy, *FEBS Lett. 385*, 53−57.
28. Hellwig, P., Behr, J., Ostermeier, C., Richter, O.-M. H., Pfitzner, U., Odenwald, A., Ludwig, B., Michel, H., and Mäntele, W. (1998) Involvement of glutamic acid 278 in the redox reaction of the cytochrome *c* oxidase from *Paracoccus denitrificans* investigated by FTIR spectroscopy, *Biochemistry 37*, 7390−7399.
29. Lübben, M., and Gerwert, K. (1996) Redox FTIR difference spectroscopy using caged electrons reveals contributions of carboxyl groups to the catalytic mechanism of haem-copper oxidases, *FEBS Lett. 397*, 303−307.
30. Yamazaki, Y., Kandori, H., and Mogi, T. (1999) Effects of subunit I mutations on redox-linked conformational changes of the *Escherichia coli bo*-type ubiquinol oxidase revealed by Fourier-transform infrared spectroscopy, *J. Biochem. (Tokyo) 126*, 194−199.
31. Lübben, M., Prutsch, A., Mamat, B., and Gerwert, K. (1999) Electron transfer induces side-chain conformational changes of glutamate-286 from cytochrome bo_3, *Biochemistry 38*, 2048−2056.
32. Hellwig, P., Soulimane, T., Buse, G., and Mäntele, W. (1999) Similarities and dissimilarities in the structure-function relation between the cytochrome *c* oxidase from bovine heart and from *Paracoccus denitrificans* as revealed by FT-IR difference spectroscopy, *FEBS Lett. 458*, 83−86.
33. Behr, J., Hellwig, P., Mäntele, W., and Michel, H. (1998) Redox dependent changes at the heme propionates in cytochrome *c* oxidase from *Paracoccus denitrificans*: Direct evidence from FTIR difference spectroscopy in combination with heme propionate ^{13}C labelling, *Biochemistry 37*, 7400−7406.
34. Dyer, R. B., Einarsdóttir, O., Killough, P. M., López-Garriga, J. J., and Woodruff, W. H. (1989) Transient binding of photodissociated CO to Cu_B^+ of eukaryotic cytochrome oxidase at ambient temperature. Direct evidence from time-resolved infrared spectroscopy, *J. Am. Chem. Soc. 111*, 7657−7659.
35. McMahon, B. H., Fabian, M., Tomson, F., Causgrove, T. P., Bailey, J. A., Rein, F. N., Dyer, R. B., Palmer, G., Gennis, R. B., and Woodruff, W. H. (2004) FTIR studies of internal proton transfer reactions linked to inter-heme electron transfer in bovine cytochrome *c* oxidase, *Biochim. Biophys. Acta 1655*, 321−331.
36. Goormaghtigh, E., Raussens, V., and Ruysschaert, J.-M. (1999) Attenuated total reflection infrared spectroscopy of proteins and lipids in biological membranes, *Biochim. Biophys. Acta 1422*, 105−185.
37. Heberle, J., and Zscherp, C. (1996) ATR/FT-IR difference spectroscopy of biological matter with microsecond time resolution, *Appl. Spectrosc. 50*, 588−596.
38. Iwaki, M., Breton, J., and Rich, P. R. (2002) ATR-FTIR difference spectroscopy of the P_M intermediate of bovine cytochrome *c* oxidase, *Biochim. Biophys. Acta 1555*, 116−121.
39. Iwaki, M., Puustinen, A., Wikström, M., and Rich, P. R. (2003) ATR-FTIR spectroscopy of the P_M and F intermediates of bovine and *Paracoccus denitrificans* cytochrome *c* oxidase, *Biochemistry 42*, 8809−8817.
40. Nyquist, R. M., Heitbrink, D., Bolwien, C., Gennis, R. B., and Heberle, J. (2003) Direct observation of protonation reactions during the catalytic cycle of cytochrome *c* oxidase, *Proc. Natl. Acad. Sci. U.S.A. 100*, 8715−8720.
41. Hellwig, P., Pfitzner, U., Behr, J., Rost, B., Pesavento, P., Donk, W.v., Gennis, R. B., Michel, H., Ludwig, B., and Mäntele, W. (2002) Vibrational modes of tyrosine in cytochrome *c* oxidase from *Paracoccus denitrificans*: FTIR and electrochemical studies on Tyr-D_4-labeled and on Tyr280His and Tyr35Phe mutant enzymes, *Biochemistry 41*, 9116−9125.
42. Schmidt, B., Hillier, W., McCracken, J., and Ferguson-Miller, S. (2004) The use of stable isotopes and spectroscopy to investigate the energy transducing function of cytochrome *c* oxidase, *Biochim. Biophys. Acta 1655*, 248−255.
43. Raitio, M., Pispa, J. M., Metso, T., and Saraste, M. (1990) Are there isoenzymes of cytochrome *c* oxidase in *Paracoccus denitrificans*? *FEBS Lett. 261*, 431−435.
44. Miller, J. H. (1992) *A Short Course in Bacterial Genetics*, Cold Spring Harbor Laboratory Press, Plainview, NY.
45. Ludwig, B. (1986) Cytochrome *c* oxidase from *Paracoccus denitrificans*, *Methods Enzymol. 126*, 153−159.
46. MacMillan, F., Kannt, A., Behr, J., Prisner, T., and Michel, H. (1999) Direct evidence for a tyrosine radical in the reaction of cytochrome *c* oxidase with hydrogen peroxide, *Biochemistry 38*, 9179−9184.
47. Riistama, S., Laakkonen, L., Wikström, M., Verkhovsky, M. I., and Puustinen, A. (1999) The calcium binding site in cytochrome aa_3 from *Paracoccus denitrificans*, *Biochemistry 38*, 10670−10677.
48. Iwaki, M., Puustinen, A., Wikström, M., and Rich, P. R. (2004) ATR-FTIR spectroscopy and isotope labeling of the P_M intermediate of *Paracoccus denitrificans* cytochrome *c* oxidase, *Biochemistry 43*, 14370−14378.

49. Glasoe, P. K., and Long, F. A. (1960) Use of glass electrodes to measure acidities in deuterium oxide, *J. Phys. Chem. 64*, 188−190.
50. Rich, P. R., and Moody, A. J. (1997) in *Bioelectrochemistry: Principles and Practice* (Gräber, P., and Milazzo, G., Eds.) pp 419−456, Birkhäuser Verlag AG, Basel, Switzerland.
51. Brunori, M., Sarti, P., Malatesta, F., Antonini, G., and Wilson, M. T. (1987) in *Cytochrome Systems: Molecular Biology and Bioenergetics* (Papa, S., Chance, B., and Ernster, L., Eds.) pp 689−695, Plenum Press, NY.
52. Moody, A. J. (1996) 'As prepared' forms of fully oxidised haem/Cu terminal oxidases, *Biochim. Biophys. Acta 1276*, 6−20.
53. Park, S., Pan, L. P., Chan, S. I., and Alben, J. O. (1996) Photoperturbation of the heme a_3-Cu_B binuclear center of cytochrome *c* oxidase CO complex observed by Fourier transform infrared spectroscopy, *Biophys. J. 71*, 1036−1047.
54. Barth, A. (2000) The infrared absorption of amino acid side chains, *Prog. Biophys. Mol. Biol. 74*, 141−173.
55. Berthomieu, C., and Hienerwadel, R. (2005) Vibrational spectroscopy to study the properties of redox-active tyrosines in photosystem II and other proteins, *Biochim. Biophys. Acta 1707*, 51−66.
56. Ayala, I., Rangel, K., York, D., and Barry, B. A. (2002) Spectroscopic properties of tyrosyl radicals in dipeptides, *J. Am. Chem. Soc. 124*, 5496−5505.
57. Rich, P. R., and Iwaki, M. (2005) in *Biophysical and Structural Aspects of Bioenergetics* (Wikström, M., Ed.) pp 314−333, Royal Society of Chemistry, Cambridge, U.K.
58. Hasegawa, K., Ono, T.-A., and Noguchi, T. (2002) Ab initio density functional theory calculations and vibrational analysis of zinc-bound 4-methylimidazole as a model of a histidine ligand in metalloenzymes, *J. Phys. Chem. A 106*, 3377−3390.
59. Hasegawa, K., Ono, T.-A., and Noguchi, T. (2000) Vibrational spectra and ab initio DFT calculations of 4-methylimidazole and its different protonation forms: Infrared and Raman markers of the protonation state of a histidine side chain, *J. Phys. Chem. B 104*, 4253−4265.
60. Gorbikova, E. A., Vuorilehto, K., Wikström, M., and Verkhovsky, M. I. (2006) Redox titration of all electron carriers of cytochrome *c* oxidase by Fourier transform infrared spectroscopy, *Biochemisry. 45*, 5641−5649.
61. Hellwig, P., Soulimane, T., Buse, G., and Mäntele, W. (1999) Electrochemical, FTIR, and UV/VIS spectroscopic properties of the ba_3 oxidase from *Thermus thermophilus*, *Biochemistry 38*, 9648−9658.
62. Gennis, R. B. (2003) Some recent contributions of FTIR difference spectroscopy to the study of cytochrome oxidase, *FEBS Lett. 555*, 2−7.
63. Kandori, H., Nakamura, H., Yamazaki, Y., and Mogi, T. (2005) Redox-induced protein structural changes in cytochrome *bo* revealed by Fourier transform infrared spectroscopy and [^{13}C]Tyr labeling, *J. Biol. Chem. 280*, 32821−32826.
64. Alben, J. O. (1978) in *The Porphyrins* (Dolphin, D., Ed.), Vol. 3, pp 323−345, Academic Press, London.
65. Han, S., Ching, Y., Hammes, S. L., and Rousseau, D. L. (1991) Vibrational structure of the formyl group on heme *a*. Implications on the properties of cytochrome *c* oxidase, *Biophys. J. 60*, 45−52.
66. Choi, S., Lee, J. J., Wei, Y. H., and Spiro, T. G. (1983) Resonance Raman and electronic spectra of heme *a* complexes of cytochrome oxidase, *J. Am. Chem. Soc. 105*, 3692−3707.
67. Berthomieu, C., Boussac, A., Mäntele, W., Breton, J., and Nabedryk, E. (1992) Molecular changes following oxidoreduction of cytochrome *b*559 characterized by Fourier transform infrared difference spectroscopy and electron paramagnetic resonance: Photooxidation in photosystem II and electrochemistry of isolated cytochrome *b*559 and iron protoporphyrin IX-bisimidazole model compounds, *Biochemistry 31*, 11460−11471.
68. Argade, P. V., Ching, Y.-C., and Rousseau, D. L. (1986) Resonance Raman spectral isolation of the *a* and a_3 chromophores in cytochrome oxidase, *Biophys. J. 50*, 613−620.
69. Ching, Y.-C., Argade, P. V., and Rousseau, D. L. (1985) Resonance Raman spectra of CN^--bound cytochrome oxidase: spectral isolation of cytochromes a^{2+}, a_3^{2+} and a_3^{2+}(CN), *Biochemistry 24*, 4938−4946.
70. Hellwig, P., Grzybek, S., Behr, J., Michel, H., and Mäntele, W. (1999) Electrochemical and ultraviolet/visible/infrared spectroscopic analysis of heme *a* and a_3 redox reactions in the cytochrome *c* oxidase from *Paracoccus denitrificans*: separation of heme *a* and a_3 contributions and assignment of vibrational modes, *Biochemistry 38*, 1685−1694.
71. Rich, P. R., and Breton, J. (2002) Attenuated total reflection Fourier transform infrared studies of redox changes in bovine cytochrome *c* oxidase: Resolution of the redox Fourier transform infrared difference spectrum of heme a_3, *Biochemistry 41*, 967−973.
72. Hu, S. Z., Smith, K. M., and Spiro, T. G. (1996) Assignment of protoheme resonance Raman spectrum by heme labeling in myoglobin, *J. Am. Chem. Soc. 118*, 12638−12646.
73. Puustinen, A., Bailey, J. A., Dyer, R. B., Mecklenburg, S. L., Wikström, M., and Woodruff, W. H. (1997) Fourier transform infrared evidence for connectivity between Cu_B and glutamic acid 286 in cytochrome bo_3 from *E. coli*, *Biochemistry 36*, 13195−13200.
74. Rost, B., Behr, J., Hellwig, P., Richter, O. M. H., Ludwig, B., Michel, H., and Mäntele, W. (1999) Time-resolved FT-IR studies on the CO adduct of *Paracoccus denitrificans* cytochrome *c* oxidase: comparison of the fully reduced and the mixed valence form, *Biochemistry 38*, 7565−7571.
75. Okuno, D., Iwase, T., Shinzawa-Itoh, K., Yoshikawa, S., and Kitagawa, T. (2003) FTIR detection of protonation/deprotonation of key carboxyl side chains caused by redox change of the Cu(A)-heme *a* moiety and ligand dissociation from the heme a_3-Cu(B) center of bovine heart cytochrome *c* oxidase, *J. Am. Chem. Soc. 125*, 7209−7218.
76. Schlereth, D. D., and Mäntele, W. (1992) Redox-induced conformational changes in myoglobin and hemoglobin: Electrochemistry and ultraviolet-visible and Fourier transform infrared difference spectroscopy at surface-modified gold electrodes in an ultra-thin-layer spectroelectrochemical cell, *Biochemistry 31*, 7494−7502.
77. Ingledew, W. J., and Rich, P. R. (2005) A study of the horseradish peroxidase catalytic cycle by FTIR spectroscopy, *Biochem. Soc. Trans. 33*, 886−889.
78. Haris, P. I., Robillard, G. T., van Dijk, A. A., and Chapman, D. (1992) Potential of ^{13}C and ^{15}N labeling for studying protein−protein interactions using Fourier transform infrared spectroscopy, *Biochemistry 31*, 6279−6284.
79. Li, T., Horan, T., Osslund, T., Stearns, G., and Arakawa, T. (1997) Conformational changes in G-CSF/receptor complex as investigated by isotope-edited FTIR spectroscopy, *Biochemistry 36*, 8849−8857.
80. Arrondo, J. L. R., Muga, A., Castresana, J., and Goñi, F. M. (1993) Quantitative studies of the structure of proteins in solution by Fourier-transform infrared spectroscopy, *Prog. Biophys. Mol. Biol. 59*, 23−56.
81. Tomson, F., Bailey, J. A., Gennis, R. B., Unkefer, C. J., Li, Z., Silks, L. A., Martinez, R. A., Donohoe, R. J., Dyer, R. B., and Woodruff, W. H. (2002) Direct infrared detection of the covalently ring linked His−Tyr structure in the active site of the heme-copper oxidases, *Biochemistry 41*, 14383−14390.
82. Cappuccio, J. A., Ayala, I., Elliot, G. I., Szundi, I., Lewis, J., Konopelski, J. P., Barry, B.A., and Einarsdóttir, Ó. (2002) Modeling the active site of cytochrome oxidase: synthesis and characterization of a cross-linked histidine-phenol, *J. Am. Chem. Soc. 124*, 1750−1760.
83. Aki, M., Ogura, T., Naruta, Y., Le, T. H., Sato, T., and Kitagawa, T. (2002) UV resonance Raman characterization of model compounds of Tyr^{244} of bovine cytochrome *c* oxidase in its neutral, deprotonated anionic, and deprotonated neutral radical forms: effects of covalent binding between tyrosine and histidine, *J. Phys. Chem. A 106*, 3436−3444.
84. McCauley, K. M., Vrtis, J. M., Dupont, J., and van der Donk, W. A. (2000) Insights into the functional role of the tyrosine-histidine linkage in cytochrome *c* oxidase, *J. Am. Chem. Soc. 122*, 2403−2404.
85. Pinakoulaki, E., Pfitzner, U., Ludwig, B., and Varotsis, C. (2002) The role of the cross-linked His-Tyr in the functional properties of the binuclear center in cytochrome *c* oxidase, *J. Biol. Chem. 277*, 13563−13568.
86. Nagano, Y., Liu, J.-G., Naruta, Y., and Kitagawa, T. (2005) UV resonance Raman study of model complexes of the Cu_B site of cytochrome *c* oxidase, *J. Mol. Struct. 735*−*736*, 279−291.
87. Wikström, M. (2004) Cytochrome *c* oxidase: 25 years of the elusive proton pump, *Biochim. Biophys. Acta 1655*, 241−247.
88. Zaslavsky, D., and Gennis, R. (2000) Proton pumping by cytochrome oxidase: progress, problems and postulates, *Biochim. Biophys. Acta 1458*, 164−179.
89. Palmer, G. (1993) Current issues in the chemistry of cytochrome *c* oxidase, *J. Bioenerg. Biomembr. 25*, 145−153.

90. Hienerwadel, R., Boussac, A., Breton, J., and Berthomieu, C. (1997) Fourier transform infrared difference spectroscopy of photosystem II tyrosine D using site-directed mutagenesis and specific isotope labeling, *Biochemistry 36*, 14712−14723.
91. Ingledew, W. J., Smith, S. M. E., Gao, Y. T., Jones, R. J., Salerno, J. C., and Rich, P. R. (2005) Ligand, cofactor, and residue vibrations in the catalytic site of endothelial nitric oxide synthase, *Biochemistry 44*, 4238−4246.
92. Pereira, M. M., Sousa, F. L., Teixeira, M., Nyquist, R. M., and Heberle, J. (2006) A tyrosine residue deprotonates during oxygen reduction by the caa_3 reductase from *Rhodothermus marinus*, *FEBS Lett. 580*, 1350−1354.
93. Fetter, J. R., Qian, J., Shapleigh, J., Thomas, J. W., García-Horsman, A., Schmidt, E., Hosler, J., Babcock, G. T., Gennis, R. B., and Ferguson-Miller, S. (1995) Possible proton relay pathways in cytochrome *c* oxidase, *Proc. Natl. Acad. Sci. U.S.A. 92*, 1604−1608.
94. Wikström, M., Jasaitis, A., Backgren, C., Puustinen, A., and Verkhovsky, M. I. (2000) The role of the D- and K-pathways of proton transfer in the function of the haem-copper oxidases, *Biochim. Biophys. Acta 1459*, 514−520.
95. Brändén, M., Sigurdson, H., Namslauer, A., Gennis, R., Ädelroth, P., and Brzezinski, P. (2001) On the role of the K-proton transfer pathway in cytochrome *c* oxidase, *Proc. Natl. Acad. Sci. U.S.A. 98*, 5013−5018.
96. Wikström, M., Verkhovsky, M. I., and Hummer, G. (2003) Water-gated mechanism of proton translocation by cytochrome *c* oxidase, *Biochim. Biophys. Acta 1604*, 61−65.
97. Michel, H. (1998) The mechanism of proton pumping by cytochrome *c* oxidase, *Proc. Natl. Acad. Sci. U.S.A. 95*, 12819−12824.
98. Rich, P. R. (2003) The molecular machinery of Keilin's respiratory chain, *Biochem. Soc. Trans. 31*, 1095−1105.

BI061114B